ACS OMEGA

http://pubs.acs.org/journal/acsodf

Article

Hydrophobic Mesoporous Silica Particles Modified With Nonfluorinated Alkyl Silanes

Chae Eun Pyo and Jeong Ho Chang*

Cite This: *ACS Omega* 2021, 6, 16100−16109

Read Online

ACCESS | Metrics & More | Article Recommendations

ABSTRACT: This work reports the preparation of hydrophobic mesoporous silica particles (MSPs) modified with nonfluorinated alkyl silanes. Alkyl silanes were grafted onto the surface of the MSPs as a function of the length of nonfluorinated alkyl chains such as propyltriethoxysilane (C_3), octyltriethoxysilane (C_8), dodecyltriethoxysilane (C_{12}), and octadecyltriethoxysilane (C_{18}). Moreover, the grafting of the different alkyl silanes onto the surface of MSPs to make them hydrophobic was demonstrated using different conditions such as by changing the pH (0, 4, 6, 8, and 13), solvent type (protic and aprotic), concentration of silanes (0, 0.12, 0.24, 0.36, 0.48, and 0.60 M), reaction time (1, 2, 3, and 4 days), and reaction temperature (25 and 40 °C). The contact angles of the alkyl silane-modified MSPs were increased as a function of the alkyl chain lengths in the order of $C_{18} > C_{12} > C_8 > C_3$, and the contact angle of C_{18}-modified MSPs was 4 times wider than that of unmodified MSPs. The unmodified MSPs had a contact angle of 25.3°, but C_{18}-modified MSPs had a contact angle of 102.1°. Furthermore, the hydrophobicity of the nonfluorinated alkyl silane-modified MSPs was also demonstrated by the adsorption of a hydrophobic lecithin compound, which showed the increase of lecithin adsorption as a function of the alkyl chain lengths. The cross-linking ratios of the modified silanes on the MSPs were confirmed by solid-state ^{29}Si-MAS nuclear magnetic resonance (NMR) measurement. Consequently, the hydrophobic modification on MSPs using nonfluorinated alkyl silanes was best preferred in a protic solvent, with a reaction time of ∼24 h at 25 °C and at a high concentration of silanes.

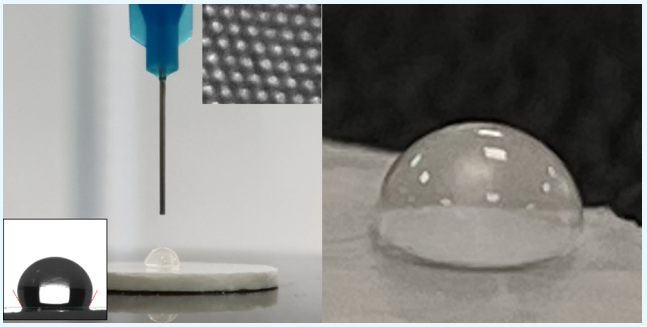

INTRODUCTION

Hydrophobic surface modification is a technology for controlling the wetting behavior of liquids on a surface, and has been used in various fields for pollution-source removal; oil−water separation; self-cleaning functions; corrosion resistance; antifouling, antifogging, and antibacterial functions; antireflective functions; and drag reductions.[1−7] Moreover, hydrophobic surface modification processes have included sol−gel, casting, lithography, electrospinning, chemical etching, chemical vapor deposition, and dip-coating.[8−14]

The hydrophobic surface modification method that has been widely used so far is the use of fluorine compounds such as poly(tetrafluoroethylene) (PTFE, Teflon) and perfluoroalkyl groups.[15−21] Because fluorine has a small atomic diameter (42 pm) and a large electronegativity (3.98), it is advantageous for lowering the surface free energy.[22−25] Stable fluorinated groups decrease the van der Waals potential with the result that electrostatic interactions limit contact between the solid and liquid phases, resulting in wider contact angles.[26] However, several recent reports have shown that the risk of the use of fluorine-based compounds involves risks of environmental contamination and human health issues such as incurable diseases (e.g., thyroid disease, cancer, and Alzheimer's syndrome), immune disorders, and hormonal disorders.[27−32] In addition, a rough-textured surface and low surface energy are required to form a hydrophobic surface. The hydrophobic surfaces are maintained by stable air pockets present in rough gaps with low surface energy. These form a barrier sheet between the droplet and the solid structure.[33] In addition, the surface energy of fluorinated compounds is the lowest among other hydrocarbon compounds, and such compounds show high stability under chemical conditions such as acidity, basicity, and heat. Consequently, they are suitable for use in various industrial fields requiring water repellency and oil repellency.[34,35]

Furthermore, many efforts have been made on the conversion of hydrophilic surfaces of mesoporous silica particles (MSPs) to hydrophobic surfaces.[36−41] The meso-

Received: April 13, 2021
Accepted: May 28, 2021
Published: June 8, 2021

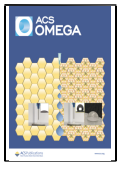

Scheme 1. Hydrophobic MSPs Using Nonfluorinated Alkyl Silanes as a Function of Alkyl Chain Lengths

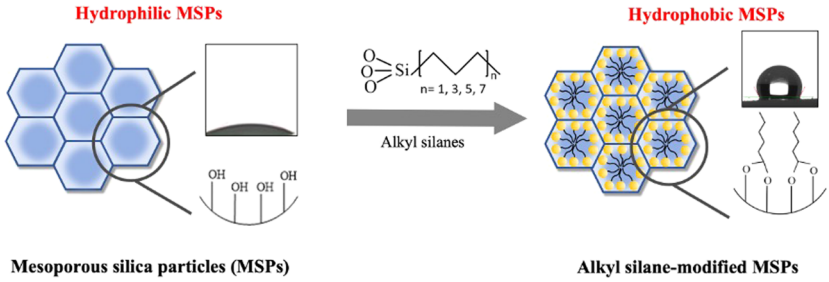

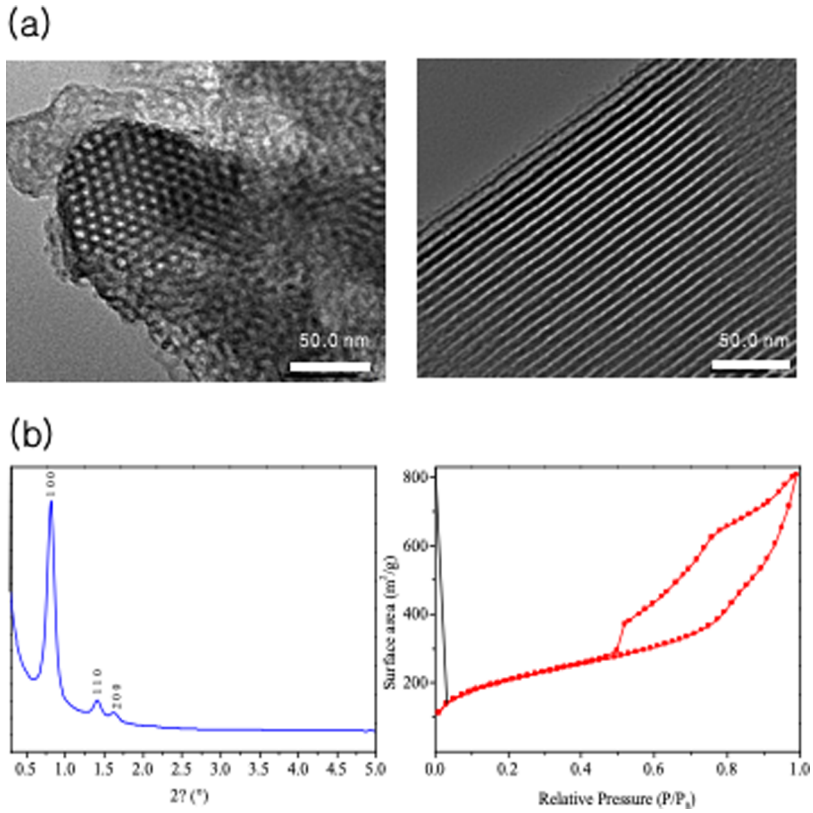

Figure 1. (a) TEM images of MSPs and (b) small-angle XRD pattern (left) and the Brunauer–Emmett–Teller (BET) isotherm (right) of MSPs.

porous silica particles (MSPs) have high surface areas (700 m^2/g or more) due to numerous silanol groups (Si–OH) in ordered nanopores and channels of 3–7 nm. For these reasons, they are used in various fields such as catalysts, scaffolds, and nanoreactors.[42−45] However, the high surface areas and abundant hydroxy groups (−OH) of MSPs are hard to be used in engineering applications involving hydrophobic surface engineering. Much of the research intended to achieve a hydrophobic surface on the MSPs has involved the use of fluorine-based silanes (or other compounds) to mask the hydroxy groups on the surface.[46,47]

In this work, we used nonfluorinated alkyl silanes for the hydrophobic surface modification on MSPs. The reason for using alkyl silanes with varying alkyl chain lengths is that the hydrophobicity increases as the length of the alkyl (C–H) chain increases. The hydrophobic MSPs were prepared by the modification with the nonfluorinated alkyl silanes as a function of the length of alkyl chains such as propyltriethoxysilane (PTES, C_3), octyltriethoxysilane (OTES, C_8), dodecyltriethoxysilane (DDTES, C_{12}), and octadecyltriethoxysilane (ODTES, C_{18}). Moreover, the hydrophobic modifications were achieved at different pH values (0–13), in different solvents (toluene and hydrochloric acid), at different silane concentrations (0.12, 0.24, 0.36, 0.48, and 0.60 M), for various reaction times (1, 2, 3, and 4 days), and at two reaction temperatures (25 and 40 °C), respectively. Furthermore, the hydrophobicity of alkyl silane-modified MSPs was achieved by hydrophobic lecithin adsorption using hydrophobic interactions between a lecithin compound and the hydrophobic mesoporous silica surfaces. Especially, solid-state ^{29}Si magic angle spinning (MAS) nuclear magnetic resonance (NMR) was used to compare the alkyl silane modification on MSPs as a function of reaction temperature (see Scheme).1

RESULTS AND DISCUSSION

Preparation and Characterization of MSPs. The characterization of the ordered MSPs such as transmission electron microscopy (TEM) images, small-angle X-ray diffraction (XRD), and N_2-adsorption and desorption isotherms is shown in Figure 1. The TEM images of the prepared

https://doi.org/10.1021/acsomega.1c01981
ACS Omega 2021, 6, 16100−16109

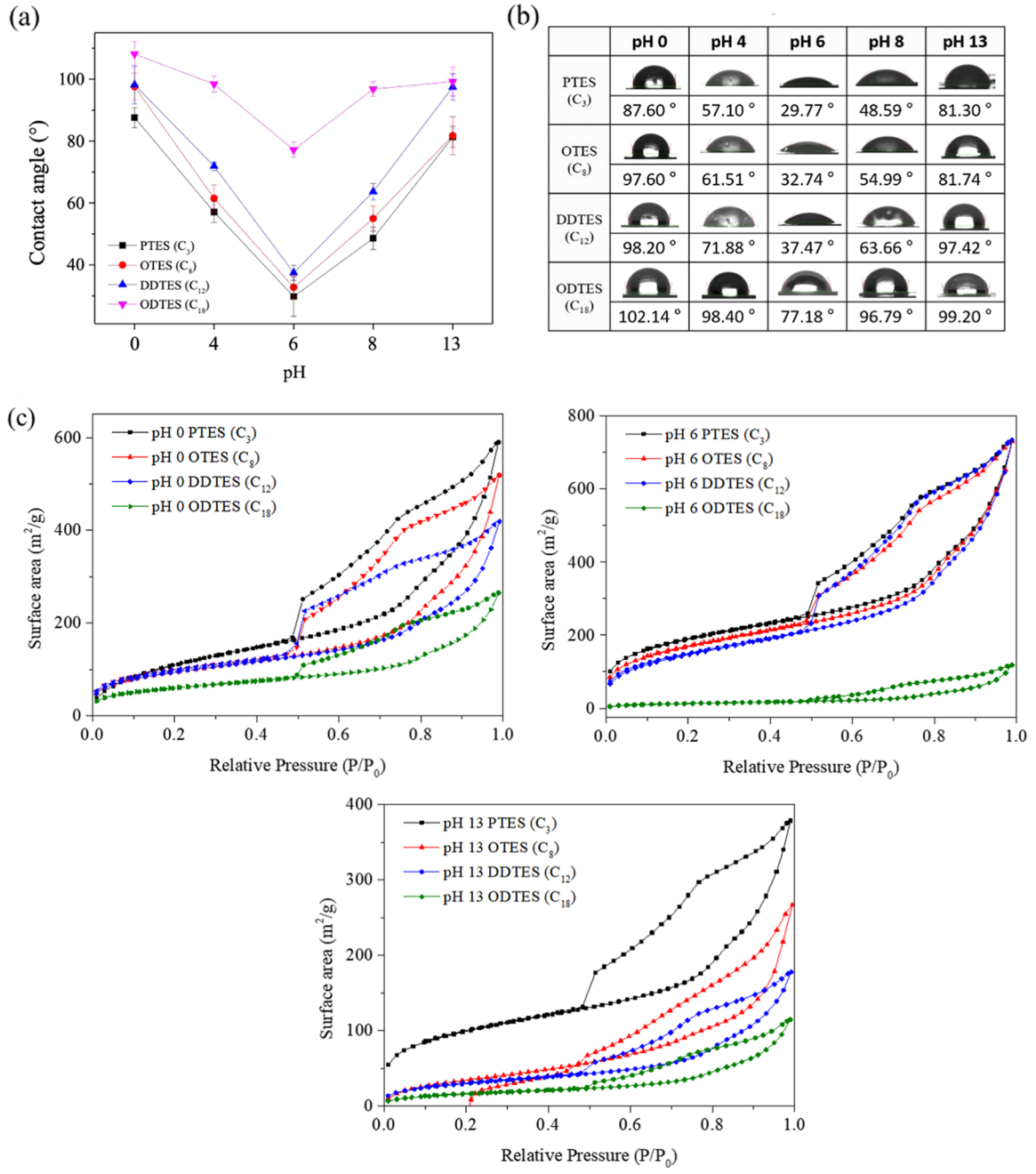

Figure 2. (a) Contact angles of the alkyl silane-modified MSPs, (b) water contact angle images, and (c) BET isotherms as a function of alkyl chain lengths at different pH values.

ordered MSPs showed a hexagonally ordered porous structure and with straight channels of 7.44 nm (Figure 1a). Moreover, small-angle XRD showed the diffractions of the ordered MSPs at 0.82, 1.41, and 1.62° of 2θ corresponding to (100), (110), and (200), respectively. N_2 adsorption−desorption isotherms of the ordered MSPs showed an H4 type hysteresis loop with a 753.16 m^2/g specific surface area (Figure 1b).

Nonfluorinated Alkyl Silane Modification of MSPs at Different pH Values. Figure 2a shows the contact angles of MSPs using alkyl silanes modified at different pH values (0, 4, 6, 8, and 13). The alkyl silane modification of the MSPs was performed as a function of the length of alkyl carbon chains (C_3, C_8, C_{12}, and C_{18}). The contact angles of MSPs modified using alkyl silanes were relatively wider when obtained under acidic and basic conditions than under neutral conditions. This means that the alkyl silane modification is a sol−gel reaction, and it is generally known that this reaction occurs well under acidic and basic conditions due to the easy protonation and deprotonation such as involved in hydrolysis and condensation.[48,49] The contact angle of the silane with the longest alkyl chain (ODTES, C_{18}) was wider than those of other alkyl silanes.

Among the ODTES-modified MSPs (the silane with the longest alkyl chain length), contact angles were 102.1, 98.4, 77.1, 96.7, and 99.2°, corresponding to pH 0, 4, 6, 8, and 13, respectively. On the other hand, contact angles of MSPs modified using PTES (C_3, the silane with the smallest alkyl chain length) were 87.6, 57.1, 29.7, 48.5, and 81.3°,

https://doi.org/10.1021/acsomega.1c01981
ACS Omega 2021, 6, 16100−16109

corresponding to pH 0, 4, 6, 8, and 13, respectively. The extent of alkyl silane modification of the MSPs indicates that more grafting occurred under acidic and basic conditions than under neutral conditions. Figure 2b shows the water contact angle images of alkyl silane-modified MSPs at different pH values (0, 4, 6, 8, and 13) as a function of the length of alkyl carbon chains (C_3, C_8, C_{12}, and C_{18}). Figure 2c shows the N_2 adsorption−desorption isotherms of alkyl silane-modified MSPs as a function of the length of alkyl carbon chains (C_3, C_8, C_{12}, and C_{18}) at pH 0, 6, and 13, respectively. With increasing length of the hydrophobic alkyl silanes used to modify the mesoporous silica surface, the surface areas were decreased and the hysteresis loop was changed to an H4 type hysteresis loop from an H3 type in lower and higher pH conditions. However, there is little change in N_2 adsorption−desorption isotherm patterns and surface areas of alkyl silane-modified MSPs except for ODTES silane modification in neutral pH conditions.

Alkyl Silane Modification of MSPs in Protic and Aprotic Solvents. Protic solvents can provide the protons needed to form new hydrogen bonds, but aprotic solvents cannot do this. Figure 3a shows a comparison of the contact angles of alkyl silane-modified MSPs in hydrochloric acid and toluene: the contact angles were wider when prepared in hydrochloric acid than in toluene. Moreover, the change in contact angles as a function of the alkyl silane modification of MSPs increased. In hydrochloric acid, the contact angles of alkyl silane-modified MSPs were increased to 87.6, 97.6, 98.2, and 102.1° as a function of the alkyl chain length (corresponding to C_3, C_8, C_{12}, and C_{18}, respectively). On the other hand, the contact angles of alkyl silane-modified MSPs as the function of alkyl chain lengths in toluene were 23.2, 50.0, 77.1, and 81.93°, respectively. Therefore, the use of protic solvents in the alkyl silane modification reaction was expected to be favorable due to their enhancement of the grafting efficiency of the alkyl silanes by an increase in the hydrolysis rate.[50,51] Figure 3b shows the correlation of contact angle measurement, surface areas, and thermogravimetric analysis (TGA) of alkyl silane-modified MSPs in hydrochloric acid. The contact angles of the alkyl silane-modified MSPs increased as a function of the alkyl chain lengths, and the contact angle of C_{18}-modified MSPs is 4 times wider than that of unmodified MSPs. The unmodified MSPs have a contact angle of 25.2°, but C_{18}-modified MSPs have a contact angle of 102.1°. As a result of the alkyl silane modification reaction, the surface areas of the alkyl silane-modified MSPs decreased to about 212.5 m^2/g from 753.1 m^2/g. The unmodified MSPs have a surface area of 753.1 m^2/g, but the alkyl silane MSPs have the surface areas of 430.5, 355.6, 334.4, and 212.5 m^2/g, corresponding to C_3, C_8, C_{12}, and C_{18}, respectively. Moreover, the grafted amounts of MSP alkyl silanes modified in hydrochloric acid increased to 12.8, 27.0, 27.8, and 33.2% as a function of the alkyl chain lengths, corresponding to C_3, C_8, C_{12}, and C_{18}, respectively. On the other hand, the grafted amounts of MSPs modified using alkyl silanes, as a function of alkyl chain lengths in toluene, were 3.92, 5.63, 6.44, and 10.30%, respectively (data are not shown). Figure 3c shows the N_2 adsorption−desorption isotherms of alkyl silane-modified MSPs as a function of the length of alkyl carbon chains (C_3, C_8, C_{12}, and C_{18}) at pH 0. With increasing length of the hydrophobic alkyl silanes used to modify the surface of MSPs, the surface areas decreased and the hysteresis loop changed to an H4 type hysteresis loop from an H3 type.

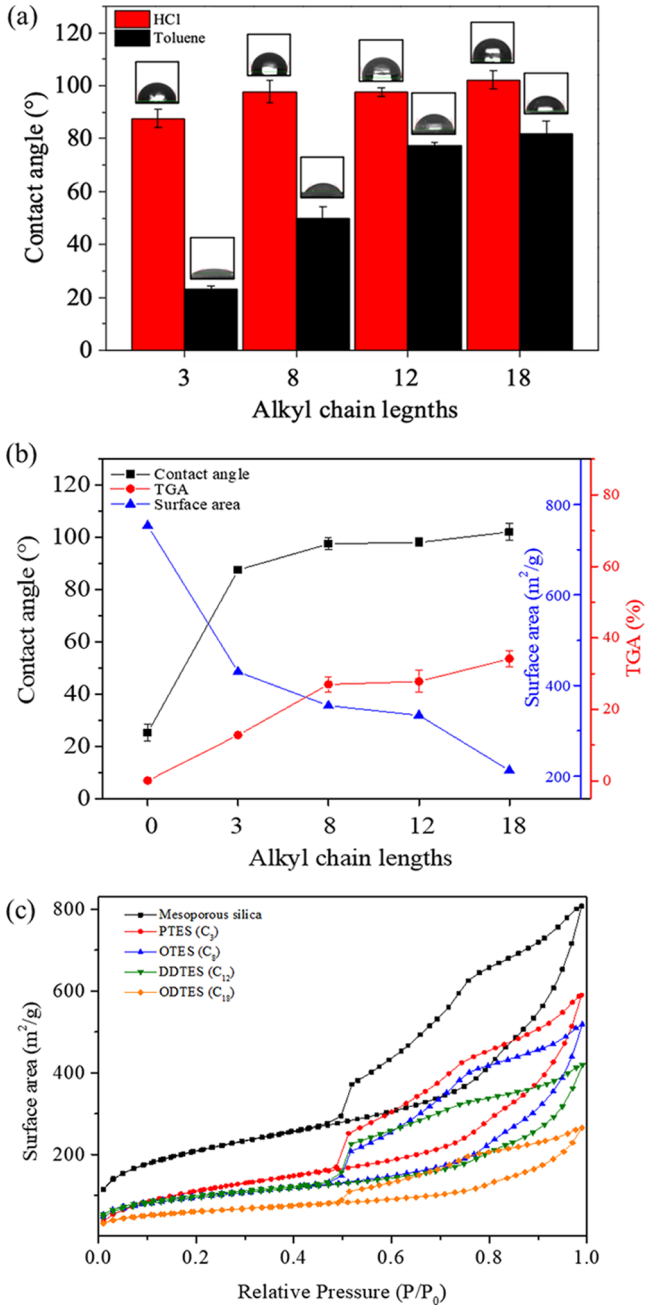

Figure 3. (a) Contact angles of the alkyl silane-modified MSPs as a function of alkyl chain lengths in different solvents (water contact angle images were inserted), (b) correlation of contact angles, surface areas, and TGA results of alkyl silane-modified MSPs as a function of alkyl chain lengths, and (c) BET isotherms as a function of alkyl chain lengths.

Modification of MSPs as a Function of the ODTES Concentration. Among the various alkyl silanes used for the surface modification of mesoporous silica, ODTES (C_{18}) had the widest contact angle regardless of the pH and the solvent used. Therefore, we demonstrated changes in the contact angle using ODTES for the modification of MSPs as the functions of the silane concentration, reaction time, and reaction temperature. Figure 4a shows the contact angles of ODTES (C_{18})-modified MSPs as a function of the silane concentration in the range 0.12−0.60 M in hydrochloric acid. With an increase in the ODTES concentration, the contact angle resulting from

https://doi.org/10.1021/acsomega.1c01981
ACS Omega 2021, 6, 16100−16109

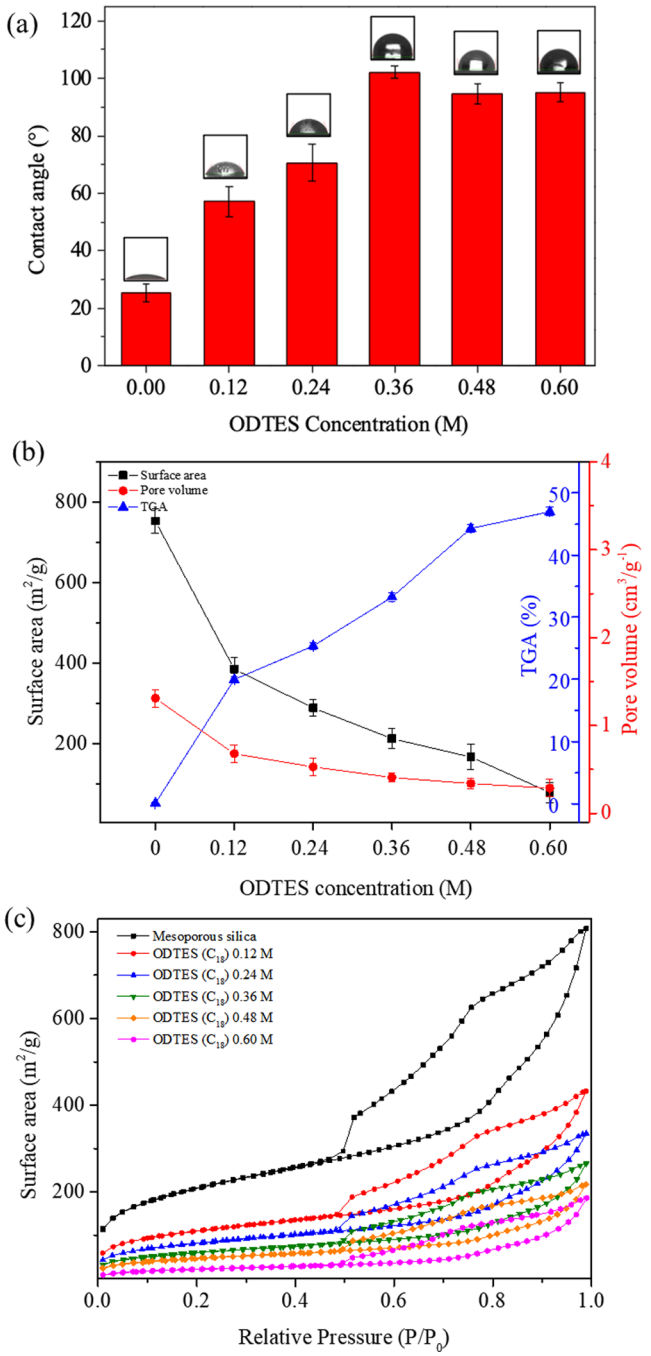

Figure 4. (a) Contact angles of the ODTES-modified MSPs as a function of the concentration, (b) correlation of the surface area, pore volume, and TGA results of the ODTES-modified MSPs as a function of the concentration, and (c) BET isotherms as a function of the concentration.

the ODTES modification of the MSPs increased in the range from 57.1 to 102.1° from the original 25.2°. Images of the contact angle as a function of the ODTES concentration are shown. Figure 4b shows the correlation of the surface area, pore volume, and thermogravimetric analysis results of ODTES-modified MSPs as a function of the silane concentration in hydrochloric acid. As the ODTES concentration used for the hydrophobic modification of the MSPs increased, the surface areas of the ODTES-modified MSPs decreased from 753.1 m^2/g of mesoporous silica to 385.1, 289.1, 212.5, 167.1, and 79.0 m^2/g, corresponding to 0.12, 0.24, 0.36, 0.48, and 0.60 M, respectively. Moreover, the grafted amounts of ODTES-modified MSPs increased to 19.9, 25.3, 33.2, 44.3, and 46.9% as a function of the ODTES concentration, corresponding to 0.12, 0.24, 0.36, 0.48, and 0.60 M, respectively.

The pore volumes of the ODTES-modified MSPs decreased from 1.31 cm^3/g of mesoporous silica to 0.68, 0.53, 0.41, 0.34 and 0.29 cm^3/g as a function of the ODTES concentration (corresponding to 0.12, 0.24, 0.36, 0.48, and 0.60 M, respectively). Figure 4c shows the N_2 adsorption−desorption isotherms of alkyl silane-modified MSPs as a function of the ODTES concentration (0, 0.12, 0.24, 0.36, 0.48, and 0.60 M) at pH 0. As the ODTES concentration increased, the surface areas decreased and the hysteresis loop changed to an H4 type hysteresis loop from an H3 type.

ODTES Modification of MSPs as a Function of the Reaction Time. To compare the relationship between the contact angle of ODTES-modified MSPs and the reaction time, the modification of the MSPs was demonstrated over 4 days with monitoring conducted every day. Figure 5a shows the contact angles of ODTES (C_{18})-modified MSPs as a function of the reaction time for 4 days. As the reaction time increased, the contact angle of the ODTES-modified MSPs slightly decreased to 102.1, 105.0, 105.4, and 111.8°, corresponding to 1, 2, 3, and 4 days, respectively. Images of the contact angles as a function of the reaction time are also shown. Figure 5b shows the correlation of the surface area, pore volume, and thermogravimetric analysis results of ODTES-modified MSPs as a function of the reaction time. Despite the increase of the reaction time used for ODTES modification of the MSPs, the surface areas of the ODTES-modified MSPs are similar (153.0−212.5 m^2/g). This trend is almost the same not only for the change in the specific surface area but also for the graft amounts and pore volume as a function of reaction time for ODTES modification. The grafted amounts and the pore volumes of the ODTES-modified MSPs are in the range of 33.2−39.4% and 0.41−0.34 cm^3/g, respectively.

Figure 5c shows the N_2 adsorption−desorption isotherms of alkyl silane-modified MSPs as a function of the reaction time (1, 2, 3, and 4 days) at pH 0. As the reaction time increased, the surface areas decreased and the hysteresis loop changed to an H4 type hysteresis loop from an H3 type.

ODTES Modification of MSPs as a Function of the Reaction Temperature. To elucidate the relationship between the contact angle of ODTES-modified MSPs and the reaction temperature, the modification of the MSPs was demonstrated at different temperatures (25 and 40 °C). Figure 6a shows changes in the contact angles and the graft amounts after the ODTES modification on the MSPs, where the contact angle was markedly decreased from 102.1 to 43.8° as the reaction temperature increased. However, the graft amounts of ODTES in the ODTES-modified MSPs increased from 33.24 to 44.37%. In general, it was predicted that the greater the TGA value according to the ODTES modification is (that is, the greater the amount modified), the more the contact angle would increase. Although the TGA value was relatively higher at 40 °C than at room temperature, the contact angle decreased as the temperature increased. To explain this result, we measured the change in the surface area, pore size, and pore volume of mesoporous silica according to the ODTES modification shown in Figure 6b. In the ODTES modification

https://doi.org/10.1021/acsomega.1c01981
ACS Omega 2021, 6, 16100−16109

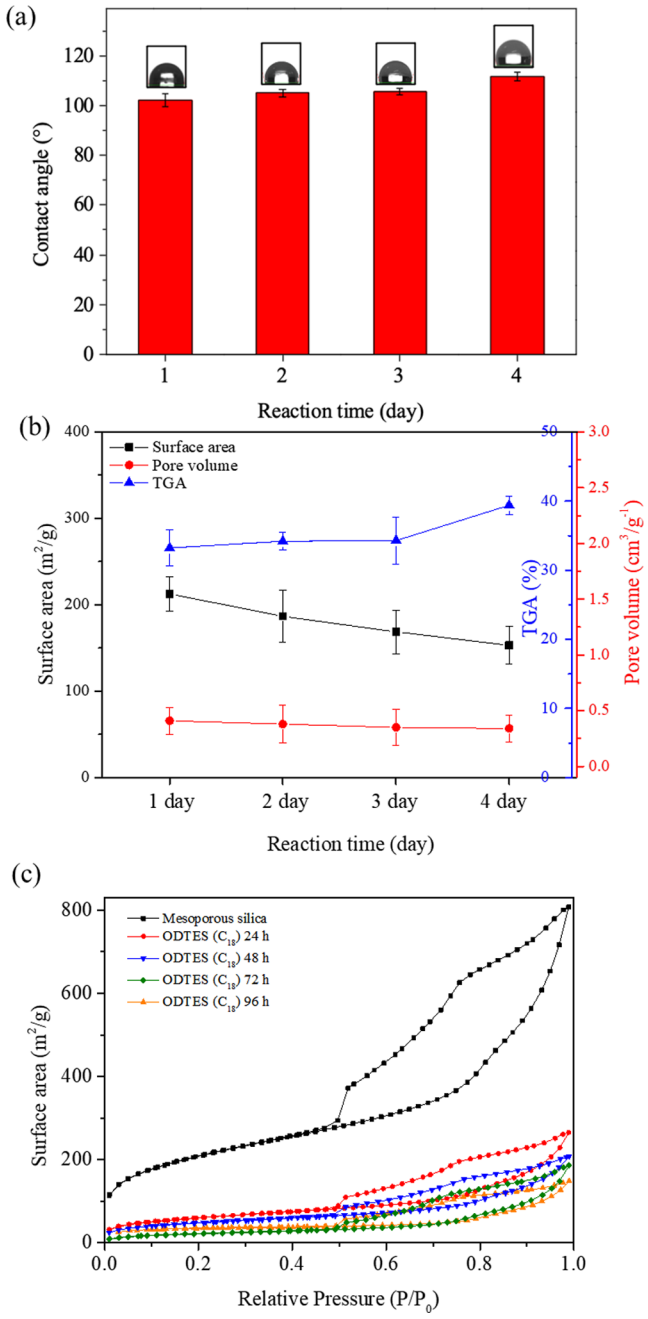

Figure 5. (a) Contact angles of the ODTES-modified MSPs as a function of the reaction time, (b) correlation of the surface area, pore volume, and TGA of the ODTES-modified MSPs as a function of the reaction time, and (c) BET isotherms as a function of the reaction time.

of mesoporous silica, the TGA value increases and the specific surface area decreases as the modification amount increases. In this work, increasing the temperature to 40 °C increased the TGA value to 44.37%, but the specific surface area also slightly increased from 97.0 to 212.5 m^2/g. However, the pore volumes of ODTES-modified MSPs decreased from 1.31 cm^3/g of MSPs to 0.41 and 0.23 cm^3/g at 25 and 40 °C, respectively.

This result can be explained by the formation of multilayer ODTES on the mesoporous surface. ODTES silanes were modified onto the MSP surfaces very quickly but were disorderly at high temperatures due to their relatively long carbon chains. ODTES silanes were also modified very rapidly (although disorderly) onto the mesoporous silica surface at 40 °C. In addition, the necessary reaction is difficult to be achieved because a monolayer forms on the mesoporous surface due to the long carbon chain. Moreover, when a large amount of ODTES was grafted onto the surface of the mesoporous silica, the ODTES formed an irregular, multilayer structure. This multilayer ODTES could reduce the pore size and pore volume of the mesoporous silica. The pore size of ODTES-modified MSPs was 7.35 and 6.95 nm at 25 and 40 °C, respectively.

Furthermore, ^{29}Si-MAS NMR spectroscopy has been extensively used to determine the bonding environment of Si atoms near the surfaces.[49] Figure 6c shows the ^{29}Si-MAS NMR spectra of ODTES-modified MSPs at 25 and 40 °C, where they show the two main peaks of T^n sites (Si−O−Si, −50 to −80 ppm) and Q^n sites (Si−OH, −90 to −130 ppm), respectively. We note that the intensities in the spectra allow qualitative estimation of the relative populations of the different T^n and Q^n sites. T^n sites of the ODTES-modified MSPs seen at −58 and −68 ppm correspond to T^2 (R-**Si**$(OSi)_2(OH)$, terminal siloxane) and T^3(R-**Si**$(OSi)_3$, cross-linking), and Q^n sites seen at −102 and −110 ppm correspond to Q^3 (**Si**-$(OSi)_3OR$) and Q^4(**Si**-$(OSi)_4$), respectively. The Q^n sites of the ODTES-modified MSPs are actually of little interest because they have the Si information on the MSP surfaces, not in the ODTES. However, we focus attention on the distribution of the surface T^n sites, which indicates the modification of ODTES silane in terminal and cross-linking sites as T^2 and T^3. It is interesting to note the degree of cross-linking when ODTES modification on MSPs is better to react at a higher temperature than at a lower temperature.

The cross-linking ratio, Si (cross-link, T^3)/Si (terminal, T^2) by the integrated analysis, is about 0.24 and 0.51 corresponding to the ODTES modification on MSPs at 25 and 40 °C, respectively. The integration of Si (Q^3) on the surface of the MSPs and the integration of Si (T^2) on the terminal of the ODTES silane showed almost constant values independent of the reaction temperature. However, the integration Si (T^3) in ODTES silane representing cross-linking was 0.124 and 0.234 when modified at 25 and 40 °C, respectively.

Moreover, the integration of Si (T^3) for all used alkyl silanes was calculated to figure out the surface density for alkyl silane-modified MSPs at room temperature. Figure 7 shows that the Si (T^3) integrations are 0.826, 0.750, 0.671, and 0.124 corresponding to C_3-MSPs, C_8-MSPs, C_{12}-MSPs, and C_{18}-MSPs, respectively. The driving force to the formation of the monolayer includes the intramolecular chain-to-chain attraction and the condensation reaction between the alkyl silanes and the silanol group in MSPs. The Si (T^3) integrations of the alkyl silanes on MSPs were decreased as a function of the alkyl chain lengths due to the steric hindrance. This is because increasing chain lengths of alkyl silanes result in steric hindrance between them, which try to anchor them on the MSP surface as far away as possible.

Lecithin Adsorption on Alkyl Silane-Modified MSPs. To elucidate the hydrophobicity of the surface of alkyl silane-modified MSPs, the lecithin compound adsorbed on each hydrophobic alkyl silane-modified MSPs. The lecithin is well known for the hydrophobic compounds so it is better adsorbed on hydrophobic surfaces than on hydrophilic surfaces by hydrophobic interaction. As a result, the adsorption efficiency of lecithin on hydrophobic alkyl silane-modified MSPs was

https://doi.org/10.1021/acsomega.1c01981
ACS Omega 2021, 6, 16100−16109

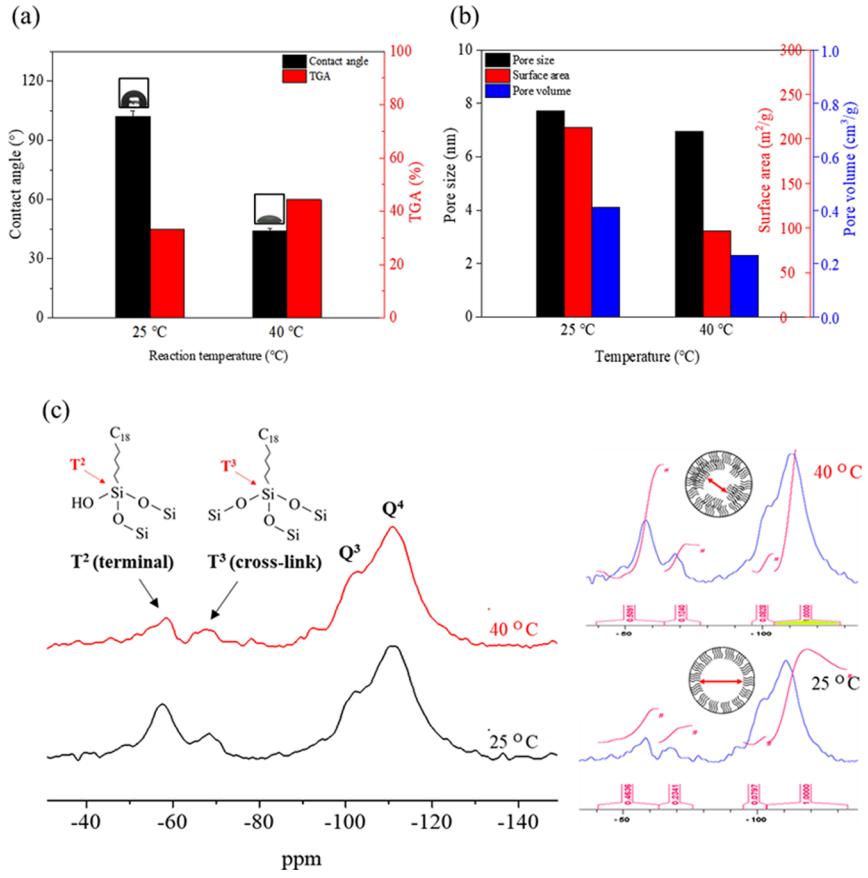

Figure 6. (a) Contact angles and TGA results, (b) correlation of the surface area, pore volume, and pore size, and (c) solid-state ^{29}Si-MAS NMR spectra include the integrated analysis as a function of the reaction temperature.

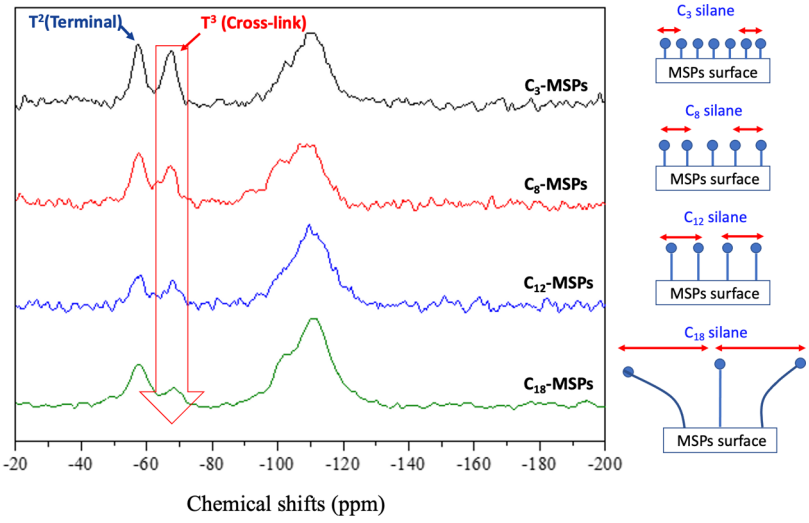

Figure 7. Solid-state ^{29}Si-MAS NMR spectra and schemes of surface packing of alkyl silane-modified MSPs.

33.12, 48.06, 58.78, 62.76, and 83.68 corresponding to MSPs, C_3-MSPs, C_8-MSPs, C_{12}-MSPs, and C_{18}-MSPs, respectively, as shown in Figure 8.

Contact Angle Comparison of Fluorinated MSPs and Nonfluorinated MSPs. To compare the contact angles of fluorinated MSPs (FMSPs) and nonfluorinated MSPs, C_3-FMSPs were prepared and the contact angles were compared with C_3-MSPs and C_{18}-MSPs, as shown in Figure 9. C_3-FMSPs and C_3-MSPs have the same length of alkyl chains, and the contact angles of C_3-FMSPs and C_3-MSPs are about 114.2 and 88.9°, respectively. It is consistent with the result that fluorinated modification showed much better hydrophobicity than nonfluorinated modification.[47] However, the contact angle increased with the increase in the alkyl chain length of the nonfluorinated silanes. The contact angle of C_{18}-MSPs was 108.1°, which is about much higher than that of C_3-MSPs, and the difference in the contact angle with C_3-FMSPs was also reduced to within 6°. Consequently, the use of nonfluorinated

https://doi.org/10.1021/acsomega.1c01981
ACS Omega 2021, 6, 16100−16109

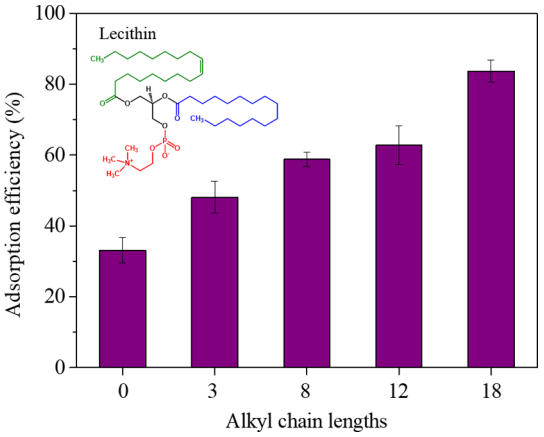

Figure 8. Adsorption efficiency of lecithin on hydrophobic alkyl silane-modified MSPs as a function of alkyl chain lengths.

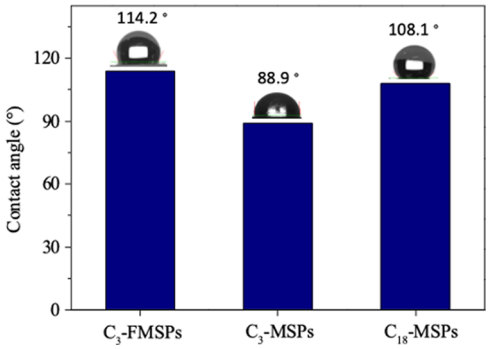

Figure 9. Contact angle comparison of C_3-FMSPs, C_3-MSPs, and C_{18}-MSPs.

alkyl silanes for hydrophobic mesoporous silica may not be superior to fluorinated alkyl silanes but it can exhibit almost similar contact angles. Furthermore, we believe that the use of nonfluorinated alkyl silanes is much safer than the use of fluorinated silanes for human safety.

CONCLUSIONS

The hydrophobic mesoporous silica particles (MSPs) were prepared by the use of nonfluorinated alkyl silanes as the function of the alkyl chain length (C_3 to C_{18}). The grafting of the different alkyl silanes onto the surface of MSPs was demonstrated using different conditions such as pH, solvent types, the concentration of silanes, reaction time, and reaction temperature. The hydrophobic contact angles of alkyl silane-modified MSPs were in the order $C_{18} > C_{12} > C_8 > C_3$, and the contact angle of C_{18}-modified MSPs was 4 times wider than that of unmodified MSPs. Furthermore, the hydrophobicity of the nonfluorinated alkyl silane-modified MSPs was also demonstrated by the adsorption of a hydrophobic lecithin compound, which showed the increase of lecithin adsorption as a function of the alkyl chain lengths due to the hydrophobic interaction. The degree of cross-linking of the modified silanes on the MSPs was confirmed by ^{29}Si-MAS NMR measurement using the terminal (T^2) and cross-linking sites (T^3) of the modified silanes. Consequently, the hydrophobic modification on the MSP surface using nonfluorinated alkyl silanes was best preferred in a protic solvent, with a reaction time of ∼24 h at 25 °C at a high concentration of silanes.

EXPERIMENTAL SECTION

Materials. Pluronic P123 (poly(ethyleneoxide)-poly-(propyleneoxide)-poly(ethyleneoxide)) was purchased from BASF (Korea). Tetraethyl orthosilicate (TEOS, >99%), potassium bicarbonate (99.5%), lecithin (98%), and ethyl alcohol anhydrous (99.9%) were purchased from Sigma-Aldrich (Korea). Propyltriethoxysilane (PTES, C_3), octyltriethoxysilane (OTES, C_8), dodecyltriethoxysilane (DDTES, C_{12}), and octadecyltriethoxysilane (ODTES, C_{18}) were purchased from Gelest (Morrisville). Acetic acid (99.5%), toluene (99.5%), hydrochloric acid, and anhydrous ethyl alcohol (99.9%) were purchased from Daejung Co. (Korea).

Preparation of the Mesoporous Silica Particles (MSPs). A portion (4.0 g) of Pluronic P123 was dissolved in 150 mL of distilled water by stirring at 40 °C for 8 h. Then, 8.5 g of TEOS was dripped into the solution at 40 °C and stirred for 24 h. This solution was put in a steel bomb and aged in a vacuum oven at 120 °C for 8 h. The remaining powder was filtered, washed with ethanol and distilled water, and dried at room temperature. A temperature of 550 °C was maintained for 6 h, and the powder was calcined.

Alkyl Silane Modification of MSPs at Different pH Values. Taking 60 mL portions of solutions at various pH values (0, 4, 6, 8, and 13), 1 g of MSPs was added to each and then stirred for 2 h. Next, 3 g of each alkyl silane (PTES, OTES, DDTES, and ODTES) was added. After stirring for 24 h, the solids were filtered, washed with ethanol, and then dried at room temperature.

Alkyl Silane Modification of MSPs in Protic and Aprotic Solvents. A total of 1 g of MSPs was added to a 60 mL portion of hydrochloric acid, and then stirred for 2 h. To each, 3 g of alkyl silane (PTES, OTES, DDTES, or ODTES) was added. After 24 h of stirring, the solids were filtered, washed with ethanol, and then dried at room temperature. Moreover, 1 g of MSPs was added to 100 mL of toluene and stirred for 2 h. After heating the solution to 60 °C, a portion (3 g) of alkyl silane (PTES, OTES, DDTES, or ODTES) was added and then refluxed for 24 h. Finally, the solids were filtered, washed with ethanol, and dried at room temperature.

ODTES Modification of MSPs as a Function of the Silane Concentration, Reaction Time, and Reaction Temperature. ODTES modification of MSPs as a function of the silane concentration was demonstrated by adding 1 g of MSPs to 60 mL of hydrochloric acid and then stirring for 2 h. ODTES at various concentrations (0.12, 0.24, 0.36, 0.48, and 0.60 M) was added to this solution. After stirring for 24 h, the solids were filtered, washed with ethanol, and then dried at room temperature. ODTES modification of MSPs as a function of the reaction time was demonstrated by adding 1 g of MSPs to 60 mL of 1 M hydrochloric acid and stirring for 2 h. Then, another portion (0.36 M) of ODTES was added to this solution. The mixture was kept for 4 days, after which the solids were filtered, washed with ethanol, and then dried at room temperature. ODTES modification of MSPs as a function of the reaction temperature was demonstrated by adding 1 g of MSPs to 60 mL of 1 M hydrochloric acid and stirring for 2 h. After heating this solution to 40 °C, 0.36 M of ODTES was added. This was stirred for 24 h; then, the solids were filtered, washed with ethanol, and dried at room temperature.

Lecithin Adsorption on Alkyl Silane-Modified MSPs. Lecithin adsorption was demonstrated on alkyl silane-modified

https://doi.org/10.1021/acsomega.1c01981
ACS Omega 2021, 6, 16100−16109

MSPs to evaluate the hydrophobicity between the hydrophobic lecithin and the hydrophobic mesoporous silica surface. A total of 1 g of mesoporous silica and alkyl silane-modified MSPs each were added to a 0.25 mM lecithin solution (in ethanol), the mixture was stirred for 24 h at room temperature, and then dried after filtration. Adsorption efficiency of lecithin on mesoporous silica and alkyl silane-modified MSPs was calculated by ultraviolet−visible (UV−vis) spectrophotometry.

Instrumental Analysis. Contact angle measurement was provided by a water contact angle analysis (WCA) using a contact angle analyzer from Git Soft Tech. Each WCA was conducted three times with 10 μL of distilled water, during which an image was taken using a digital camera. The Brunauer−Emmett−Teller (BET) analyses were performed using a Micromeritics ASAP 2420. Identification and characterization of the alkyl silane-modified MSPs were carried out by thermogravimetric analysis (TGA) and solid-state ^{29}Si magic angle spinning nuclear magnetic resonance (MAS NMR). TGA was performed using a Q600 TA instrument at a rate of 10 °C min^{-1} in N_2 gas at temperatures from 25 to 700 °C. Solid-state ^{29}Si-MAS NMR measurements were performed in a 9.4 T Bruker Ascend 400WB instrument using a 4 mm zirconia rotor with a pulse length of 1.6 μs, a spinning rate of 11 kHz, and a repetition delay of 20 s. The morphological and structural details of the MSPs were studied using field-emission scanning electron microscopy (FE-SEM) and transmission electron microscopy (TEM). The FE-SEM investigations were carried out using a Tescan Mira-3 instrument with an accelerating voltage of 2 kV. TEM was carried out on a JEOL JEM-2100 electron microscope operated at 200 kV. Small-angle and wide-angle X-ray diffraction (XRD) studies were performed using a SmartLab and a Miniflex 600 (Rigaku) with scan ranges of 1.5−5 and 10−90°, respectively.

AUTHOR INFORMATION

Corresponding Author

Jeong Ho Chang − *Korea Institute of Ceramic Engineering and Technology, Jinju, Gyeongnam 52851, Korea;* Present Address: Center for Convergence Bioceramic Materials, Korea Institute of Ceramic Engineering and Technology, Chungbuk 28160, Korea.; orcid.org/0000-0002-8222-4176; Email: jhchang@kicet.re.kr

Author

Chae Eun Pyo − *Korea Institute of Ceramic Engineering and Technology, Jinju, Gyeongnam 52851, Korea; Department of Chemical Engineering, Hanyang University, Seoul 04763, Korea*

Complete contact information is available at: https://pubs.acs.org/10.1021/acsomega.1c01981

Notes

The authors declare no competing financial interest.

ACKNOWLEDGMENTS

This work was supported by a grant from the R&D program funded by the Ministry of Trade, Industry and Energy (MOTIE, Korea), part of the Industry Core Technology Development Program funded by the Korea Evaluation Institute of Industrial Technology (KEIT) [20003970].

REFERENCES

(1) Shibuichi, S.; Onda, T.; Satoh, N.; Tsujii, K. Super water-repellent surfaces resulting from fractal structure. *J. Phys. Chem. A* **1996**, *100*, 19512−19517.

(2) Teli, M. D.; Annaldewar, B. N. Superhydrophobic and ultraviolet protective nylon fabrics by modified nano silica coating. *J. Text. Inst.* **2017**, *108*, 460−466.

(3) Gor, P. M.; Balakrishnan, S.; Kandasubramanian, B. Super-hydrophobic Corrosion Inhibition Polymer Coatings. In *Super-hydrophobic Polymer Coatings*; Elsevier, 2009; pp 223−243.

(4) Kwak, G.; Lee, M.; Senthil, K.; Yong, K. Wettability control and water droplet dynamics on SiC-SiO_2 core-shell nanowires. *Langmuir* **2010**, *26*, 12273−12277.

(5) Jayan, J. S.; Jayadev, D.; Pillai, Z. S.; Joseph, K. et al. The Stability of the Superhydrophobic Surfaces. *Superhydrophobic Polymer Coatings*, 2019; pp 123−159.

(6) Hozumi, A.; Urata, C. Development of environmentally-friendly surface modification technology. *Synthesiology* **2014**, *7*, 190−198.

(7) Qu, M.; Yuan, M.; Liu, S.; He, J.; Xue, M.; Liu, X.; Li, S.; et al. A versatile and efficient method to fabricate recyclable superhydrophobic composites based on brucite and organosilane. *J. Mater. Sci.* **2018**, *53*, 396−408.

(8) Zhang, P.; Lv, F. Y. A review of the recent advances in superhydrophobic surfaces and the emerging energy-related applications. *Energy* **2015**, *82*, 1068−1087.

(9) Dey, T.; Naughton, D. Cleaning and anti-reflective (AR) hydrophobic coating of glass surface: a review from materials science perspective. *J. Sol−Gel Sci. Technol.* **2016**, *77*, 1−27.

(10) Valipour, M. N.; Birjandi, F. C.; Sargolzaei, J. Super-non-wettable surfaces: A review. *Colloids Surf., A* **2014**, *448*, 93−106.

(11) Zhang, M.; Feng, S.; Wang, L.; Zheng, Y. Lotus effect in wetting and self-cleaning. *Biotribology* **2016**, *5*, 31−43.

(12) Li, Y.; Men, X.; Zhu, X.; Ge, B.; Chu, F.; Zhang, Z. One-step spraying to fabricate nonfluorinated superhydrophobic coatings with high transparency. *J. Mater. Sci.* **2016**, *51*, 2411−2419.

(13) Kumar, S.; Malik, M. M.; Purohit, R. Synthesis methods of mesoporous silica materials. *Mater. Today: Proc.* **2017**, *4*, 350−357.

(14) Ellinas, K.; Tserepi, A.; Gogolides, E. From super-amphiphobic to amphiphilic polymeric surfaces with ordered hierarchical roughness fabricated with colloidal lithography and plasma nanotexturing. *Langmuir* **2011**, *27*, 3960−3969.

(15) Teli, M. D.; Annaldewar, B. N. Superhydrophobic and ultraviolet protective nylon fabrics by modified nano silica coating. *J. Text. Inst.* **2017**, *108*, 460−466.

(16) Yu, M.; Gu, G.; Meng, W. D.; Qing, F. L. Superhydrophobic cotton fabric coating based on a complex layer of silica nanoparticles and perfluorooctylated quaternary ammonium silane coupling agent. *Appl. Surf. Sci.* **2007**, *253*, 3669−3673.

(17) Pagliaro, M.; Ciriminna, R. New fluorinated functional materials. *J. Mater. Chem.* **2005**, *15*, 4981−4991.

(18) Cai, Y.; Zhao, Q.; Quan, X.; Feng, W.; Wang, Q. Fluorine-free and hydrophobic hexadecyltrimethoxysilane-TiO_2 coated mesh for gravity-driven oil/water separation. *Colloids Surf., A* **2020**, *586*, No. 124189.

(19) Zhang, J.; Li, J.; Han, Y. Superhydrophobic PTFE surfaces by extension. *Macromol. Rapid Commun.* **2004**, *25*, 1105−1108.

(20) Gao, L.; J M Carthy, T. Teflon is hydrophilic. Comments on definitions of hydrophobic, shear versus tensile hydrophobicity, and wettability characterization. *Langmuir* **2008**, *24*, 9183−9188.

(21) Baghel, V.; Sikarwar, B. S.; Pachchigar, V.; Ranjan, M. Moist air condensation on Teflon coated copper helical coil. *Mater. Today: Proc.* **2021**, *38*, 397−401.

(22) Hird, M. Fluorinated liquid crystals–properties and applications. *Chem. Soc. Rev.* **2007**, *36*, 2070−2095.

(23) Tiwari, P.; Gupta, A.; Mehra, R. R.; Khan, N.; Harjit, J.; Basu, A.; Tiwari, A.; Singh, M.; Konar, A. D.; et al. Fluorinated diphenylalanine analogue based supergelators: a stencil that accentuates the sustained release of antineoplastic drugs. *Supramol. Chem.* **2020**, *32*, 495−507.

(24) Ye, L.; Xie, Y.; Weng, K.; Ryu, H. S.; Li, C.; Cai, Y.; Fu, H.; Wei, D.; Woo, H. Y.; Tan, S.; Sun, Y. Insertion of chlorine atoms onto π-bridges of conjugated polymer enables improved photovoltaic performance. *Nano Energy* **2019**, *58*, 220−226.
(25) Teshima, K.; Sugimura, H.; Inoue, Y.; Takai, O.; Takano, A. Ultra-Water-Repellent (Polyethylene terephthalate) Substrates. *Langmuir* **2003**, *19*, 10624−10627.
(26) Janowicz, N. J.; Li, H.; Heale, F.; Parkin, I.; Papakonstantinou, I.; Tiwari, M. K.; Carmalt, C. J. Fluorine-Free Transparent Superhydrophobic Nanocomposite Coatings from Mesoporous Silica. *Langmuir* **2020**, *36*, 13426−13438.
(27) Wankhede, R. G.; Shantaram; Thanawala, K.; Khanna, A.; Birbillis, N. Development of Hydrophobic Non-Fluorine Sol-Gel Coatings on Aluminium Using Long Chain Alkyl Silane Precursor. *J. Mater. Sci. Eng.* **2013**, *3*, 224−331.
(28) Saharudin, K. A.; Sreekantan, S.; Basiron, N.; Chun, L. K.; Kumaravel, V.; Abdullah, T. K.; Ahmad, Z. A. Improved superhydrophobicity of eco-friendly coating from palm oil fuel ash (POFA) waste. *Surf. Coat. Technol.* **2018**, *337*, 126−135.
(29) Xue, C. H.; Li, Y. R.; Zhang, P.; Ma, J. Z.; Jia, S. T. Washable and Wear-Resistant Superhydrophobic Surfaces with Self-Cleaning Property by Chemical Etching of Fibers and Hydrophobization. *ACS Appl. Mater. Interfaces* **2014**, *6*, 10153−10161.
(30) Cui, L.; Zhou, Q. F.; Liao, C. Y.; Fu, J. J.; Jiang, G. B. Studies on the Toxicological Effects of PFOA and PFOS on Rats Using Histological Observation and Chemical Analysis. *Arch. Environ. Contam. Toxicol.* **2009**, *56*, 338−349.
(31) da Silva, Í. G. M. D.; Lucas, E. F.; Advincula, R. Fluorine-Free Superhydrophobic Coatings: Rapid Fabrication and Highly Efficient Oil/Water Separation. *Macromol Mater. Eng.* **2020**, No. 2000400.
(32) Guan, X.; He, M.; Chang, J.; Wang, Z.; Chen, Z.; Fan, H. Photo-controllability of fluoride remediation by spiropyran-functionalized mosoporous silica powder. *J. Environ. Chem. Eng.* **2020**, No. 104655.
(33) Monde, T.; Fukube, H.; Nemoto, F.; Yoko, T.; Konakahara, T. Preparation and surface properties of silica-gel coating films containing branched-polyfluoroalkylsilane. *J. Non-Cryst. Solids* **1999**, *246*, 54−64.
(34) Venkateswara Rao, A.; Latthe, S. S.; Nadargi, D. Y.; Hirashima, H.; Ganesan, V. Preparation of MTMS based transparent superhydrophobic silica films by sol−gel method. *J. Colloid Interface Sci.* **2009**, *332*, 484−490.
(35) Rice, B. L.; Guo, C. Y.; Kirchmeier, R. L. Perfluorocarbon Phosphonic and Sulfonic Acids Containing Discretely Varying Terminal Functional Groups. *Inorg. Chem.* **1991**, *30*, 4635−4638.
(36) Wang, T.; Wang, Y.; Liao, C.; Cai, Y.; Jiang, G. Perspectives on the Inclusion of Perfluorooctane Sulfonate into the Stockholm Convention on Persistent Organic Pollutants. *Environ. Sci. Technol.* **2009**, *43*, 5171−5175.
(37) Anitha, C.; Azim, S. S.; Mayavan, S. Fluorine free superhydrophobic surface textured silica particles and its dynamics−Transition from impalement to impingement. *J. Alloys Compd.* **2017**, *711*, 197−204.
(38) Bayer, I. S. Superhydrophobic Coatings from Ecofriendly Materials and Processes: A Review. *Adv. Mater. Interfaces* **2020**, *7*, No. 2000095.
(39) Jeevajothi, K.; Subasri, R.; Raju, K. R. C. S. Transparent, non-fluorinated, hydrophobic 9silica coatings with improved mechanical properties. *Ceram. Int.* **2013**, *39*, 2111−2116.
(40) Li, S.; Jiao, X.; Yang, H. Hydrophobic Core/Hydrophilic Shell Structured Mesoporous Silica Nanospheres: Enhanced Adsorption of Organic Compounds from Water. *Langmuir* **2013**, *29*, 1228−1237.
(41) Lahiri, S. K.; Zhang, P. Z.; Zhang, C.; Liu, L. Robust Fluorine-Free and Self-Healing Superhydrophobic Coatings by H_3BO_3 Incorporation with SiO_2-Alkyl-Silane@PDMS on Cotton Fabric. *ACS Appl. Mater. Interfaces* **2019**, *11*, 10262−10275.
(42) Wang, T.; Bao, T.; Gao, Z.; Wu, Y.; Wu, L. Synthesis of mesoporous silica-shell/oil-core microspheres for common water-borne polymer coatings with robust superhydrophobicity. *Prog. Org. Coat.* **2019**, *132*, 275−282.
(43) Douroumis, D.; Onyesom, I.; Maniruzzaman, M.; Mitchell, J. Mesoporous silica nanoparticles in nanotechnology. *Crit. Rev. Biotechnol.* **2013**, *33*, 229−245.
(44) Huang, X.; Teng, X.; Chen, D.; Tang, F.; He, J. The effect of the shape of mesoporous silica nanoparticles on cellular uptake and cell function. *Biomaterials* **2010**, *13*, 438−448.
(45) Huang, D.-M.; Chung, T. H.; Hung, Y.; Lu, F.; Wu, S. H.; Mou, C. Y.; Yao, M.; Chen, Y. C. Internalization of mesoporous silica nanoparticles induces transient but not sufficient osteogenic signals in human mesenchymal stem cells. *Toxicol. Appl. Parmacol.* **2008**, *231*, 208−215.
(46) Lee, J.; Lee, S. Y.; Park, S.; Chang, J. H. In *Histidine-Tagged Enzyme Conjugated Heterogeneous Magnetic Mesoporous Silica for Highly Efficient Biodegradation of Catechol*, 2011 IEEE Nanotechnology Materials and Devices Conference, 2011; pp 450−451.
(47) Lee, S. Y.; Lee, J. H.; Chang, J. H.; Lee, J. H. Inorganic nanomaterial-based biocatalysts. *BMB Rep.* **2011**, *44*, 77−86.
(48) Acres, R. G.; Ellis, A. V.; Alcino, J.; Lenahan, C. E.; Khodakov, D. A.; Metha, G. F.; Andersson, G. G. Molecular Structure of 3-Aminopropyltriethoxysilane Layers Formed on Silanol-Terminated Silicon Surfaces. *J. Phys. Chem. C.* **2012**, *116*, 6289−6297.
(49) Liu, J.; Shin, Y. S.; Nie, Z.; Chang, J. H.; Wang, L. Q.; Fryxell, G. E.; Samuel, W. D.; Exarhos, G. J. Molecular Assembly in Ordered Mesoporosity: A New Class of Highly Functional Nanoscale Materials. *J. Phys. Chem. A* **2000**, *104*, 8328−8339.
(50) Attinger, D.; Frankiewicz, C.; Betz, A. R.; Schutzius, T. M.; Gangult, R.; Das, A.; Kim, C. J.; Megaridis, C. M. Surface engineering for phase change heat transfer: A review. *MRS Energy Sustainability* **2014**, *1*, No. 4.
(51) He, M.; Wang, J.; Li, H.; Song, Y. Super-hydrophobic surfaces to condensed micro-droplets at temperatures below the freezing point retard ice/frost formation. *Soft Matter* **2011**, *7*, 3993−4000.

https://doi.org/10.1021/acsomega.1c01981
ACS Omega 2021, 6, 16100−16109